

RESEARCH

Open Access



# Kinase inhibitor pulldown assay (KiP) for clinical proteomics

Alexander B. Saltzman<sup>1†</sup>, Doug W. Chan<sup>2,5†</sup>, Matthew V. Holt<sup>2†</sup>, Junkai Wang<sup>2,3</sup>, Eric J. Jaehnig<sup>2</sup>, Meenakshi Anurag<sup>2</sup>, Purba Singh<sup>2,7</sup>, Anna Malovannaya<sup>1,4</sup>, Beom-Jun Kim<sup>2,6\*</sup> and Matthew J. Ellis<sup>2\*</sup>

## Abstract

Protein kinases are frequently dysregulated and/or mutated in cancer and represent essential targets for therapy. Accurate quantification is essential. For breast cancer treatment, the identification and quantification of the protein kinase ERBB2 is critical for therapeutic decisions. While immunohistochemistry (IHC) is the current clinical diagnostic approach, it is only semiquantitative. Mass spectrometry-based proteomics offers quantitative assays that, unlike IHC, can be used to accurately evaluate hundreds of kinases simultaneously. The enrichment of less abundant kinase targets for quantification, along with depletion of interfering proteins, improves sensitivity and thus promotes more effective downstream analyses. Multiple kinase inhibitors were therefore deployed as a capture matrix for kinase inhibitor pulldown (KiP) assays designed to profile the human protein kinome as broadly as possible. Optimized assays were initially evaluated in 16 patient derived xenograft models (PDX) where KiP identified multiple differentially expressed and biologically relevant kinases. From these analyses, an optimized single-shot parallel reaction monitoring (PRM) method was developed to improve quantitative fidelity. The PRM KiP approach was then reapplied to low quantities of proteins typical of yields from core needle biopsies of human cancers. The initial prototype targeting 100 kinases recapitulated intrinsic subtyping of PDX models obtained from comprehensive proteomic and transcriptomic profiling. Luminal and HER2 enriched OCT-frozen patient biopsies subsequently analyzed through KiP-PRM also clustered by subtype. Finally, stable isotope labeled peptide standards were developed to define a prototype clinical method. Data are available via ProteomeXchange with identifiers PXD044655 and PXD046169.

<sup>†</sup>Alexander B. Saltzman, Doug W. Chan and Matthew V. Holt have contributed equally to this work.

\*Correspondence:

Beom-Jun Kim  
beom-jun.kim@astrazeneca.com  
Matthew J. Ellis  
matthewjcellis@gmail.com

Full list of author information is available at the end of the article



© The Author(s) 2024. **Open Access** This article is licensed under a Creative Commons Attribution 4.0 International License, which permits use, sharing, adaptation, distribution and reproduction in any medium or format, as long as you give appropriate credit to the original author(s) and the source, provide a link to the Creative Commons licence, and indicate if changes were made. The images or other third party material in this article are included in the article's Creative Commons licence, unless indicated otherwise in a credit line to the material. If material is not included in the article's Creative Commons licence and your intended use is not permitted by statutory regulation or exceeds the permitted use, you will need to obtain permission directly from the copyright holder. To view a copy of this licence, visit <http://creativecommons.org/licenses/by/4.0/>. The Creative Commons Public Domain Dedication waiver (<http://creativecommons.org/publicdomain/zero/1.0/>) applies to the data made available in this article, unless otherwise stated in a credit line to the data.

## Introduction

Protein and lipid kinases are enzymatic proteins that initiate and propagate signaling cascades to drive a wide range of cancer-relevant biological functions [1]. Many cancers are driven by aberrant kinase activity, and direct therapeutic inhibition of oncogenic kinases has proven to be effective for patients where individual driving kinases can be diagnosed—often through the presence of a genomic aberration [2–4]. The full scope of both regulation and downstream consequences of dysregulated kinase abundance and activity is not fully understood. Extensive crosstalk and functional redundancies of kinase-dependent dynamic signaling processes confounds therapeutic efficacy [5]. Consequently, while kinase inhibitors can successfully induce response and promote progression-free survival, overall survival improvements has proved more challenging (PMC2880454). The development of more effective kinome-based strategies therefore requires the accurate quantification of the kinome more broadly in human biopsy samples. Preclinical models can never cover the vast heterogeneity that exists in kinase function across cancers or link kinase expression to clinical outcomes.

Mass spectrometry-based comprehensive proteomics typically requires enrichment and/or prefractionation to effectively characterize low abundance kinases [6]. Deep-coverage proteomic approaches achieve this goal through multiplexing with isobaric tags and pre-fractionation [7]. However, these approaches are cumbersome and impractical in a clinical setting where rapid data return is critical. Many kinases are not present in high abundance and are therefore more difficult to measure accurately. Furthermore, diagnostic clinical specimens present challenges in terms of the protein yields required for comprehensive kinome coverage. The development of methodologies to enrich kinases present in clinical samples is therefore also a critical endeavor.

Current enrichment strategies involve either antibodies or a kinobead approach [8–14]. Immobilized kinase inhibitors have already been used to quantify low abundance kinases [8]. These approaches can utilize inhibitors with high specificity [14] or with a broad affinity [15], as all type 1 kinase inhibitors bind the conserved ATP binding pocket domain of their targets, they can be used as an inhibitor-based affinity matrix for kinase enrichment in clinical samples. Extensive characterization of drug-kinase interactions has been performed with kinobeads [13], and specific combinations of kinobeads have been designed to maximize kinome coverage [14]. Kinase activity has been further assessed using a competitive binding assay by the addition of unbound drug. However, these approaches typically use milligram quantities (~5 mg) and their potential for tumor subtyping,

characterization and risk-stratification has not been extensively evaluated [16].

In this study we developed a kinase inhibitor pull-down assay (KiP) with clinically relevant inhibitors that is optimized for microgram protein yields typical for needle core biopsy samples. We establish the coverage and quantitative fidelity of the assay for kinases in a single-shot discovery approach. From these data we optimized a one hundred kinase targeted panel and determined the effectiveness of KiP in subtyping breast cancer patient-derived xenograft models and two breast cancer patient sample cohorts.

## Materials and methods

### Cell lines

Human melanoma cell lines SK-MEL-5 and MALME-3 M were provided by Dr. Elizabeth Grimm (MD Anderson Cancer Center) and human leukemia cell line HL-60 and human prostate cancer cell line PC-3 were provided by Dr. Margaret Goodell and Dr. Jianming Xu (Baylor College of Medicine), respectively. Breast cancer cell lines T-47D and BT-474 were obtained from the American Type Culture Collection (Rockville, MD) and WHIM12 cell line was extracted from WHIM12 PDX tumor [17]. SK-MEL-5 and MALME-3 M cell lines were maintained in DMEM medium supplemented with 10% fetal bovine serum (FBS, Sigma-Aldrich, F2442) and HL-60, PC-3, and T-47D cells were cultured in RPMI-1640 supplemented with 10% FBS. BT-474 cells were cultured in DMEM/F12 medium supplemented with 5% FBS and 5 µg/ml insulin. WHIM12 cells were cultured in Ham's F-12 medium containing 5% FBS with antibiotic and supplements (50 ng/mL sodium selenite, 50 µg/mL 3,3',5-triiodo-L-thyronine, 5 µg/mL transferrin, 5 mM ethanolamine, 1 µg/mL hydrocortisone, 5 µg/mL insulin, 10 ng/mL Epidermal growth factor, and 2 mM L-glutamine).

### PDX tumor and cell lysates preparation

Patient derived xenografts (PDX) mice studies were carried out within the recommended guidelines for care and use of laboratory animals by the National Institutes of Health. All animal procedures were approved by the Institutional Animal Care and Use Committee (IACUC) at Baylor College of Medicine (Houston, TX) under animal protocol number AN-6934.

Frozen PDX tumors were cryopulverized with a Covaris CP02 Pulverizer and resuspended in lysis buffer containing 50 mM HEPES (pH 7.5), 0.5% Triton X-100, 150 mM NaCl, 1 mM EDTA, 1 mM EGTA, 1X protease inhibitor cocktail (Roche), 10 mM NaF, 2.5 mM Na<sub>3</sub>VO<sub>4</sub> and 1% each of phosphatase inhibitor cocktails 2 and 3 (Sigma) and set on ice for 10 min prior to sonication. Cell

lysates were sonicated in a Covaris S220 sonicator for 2 min at 4 °C with settings at 100 peak power, 10 duty factor and 500 cycles/burst. Cell lysates were clarified by centrifugation at 100,000×g for 30 min at 4 °C with a Beckman Optima Ultracentrifuge. Protein concentration was determined by Bradford assay (Bio-Rad).

For cell extracts, the cell lines were grown to approximately 80% confluency and harvested by scraping in cold PBS. The cell pellets were resuspended in lysis buffer and processed in the same way as the PDX tumor samples.

#### **Kinase inhibitors**

Palbociclib, Crizotinib, GSK690693 and AZD4547 were purchased from Selleckchem. Purvalanol B and CZC-8004 were purchased from Med Chem 101. Modified Afatinib, FRAX597, Abemaciclib, and Axitinib (containing an amino side chain for coupling) were custom synthesized by Med Chem 101 (Fig. 1A and Additional file 1: Figure S1A).

#### **Kinobeads preparation**

Kinase inhibitors Palbociclib, Crizotinib, GSK690693, AZD4547, CZC-8004, Afatinib, FRAX597, Abemaciclib and Axitinib were conjugated to ECH Sepharose 4B (GE Healthcare) via carbodiimide coupling chemistry as previously described [10]. For conjugation of the nine drugs with the reactive amine group, ECH Sepharose 4B (GE Healthcare) were used up to 2017, when this reagent was discontinued by the manufacturer. We synthesized our own ECH Sepharose 4B by conjugating 6-Aminohexanoic acid (Sigma) to cyanogen bromide (CNBr)-activated Sepharose 4B (GE Healthcare) according to manufacturer's recommendation. Briefly, excess 6-Aminohexanoic acid was coupled to swollen CNBr-activated Sepharose 4B in 0.1 M NaHCO<sub>3</sub>, pH 8.3 and 500 mM NaCl at 4 °C overnight with rotation. Unreacted CNBr groups were then inactivated by incubating the beads with 0.1 M Tris-HCl pH 8.0 for 2 h. The beads were

then washed with five cycles of alternating low pH buffer (0.1 M sodium acetate, pH 4.0 with 500 mM NaCl) and high pH buffer (0.1 M Tris-HCl, pH 8.0 with 500 mM NaCl). Conjugation of the drugs to the "homemade" ECH Sepharose 4B were performed according to protocol described by Duncan et al. [10]. Briefly, the beads were conditioned by multiple washes with 50% dimethylformamide/ethanol (DMF/EtOH). Each drug was dissolved in 50% DMF/EtOH and added to the conditioned beads in the presence of 0.1 M 1-ethyl-3-(3-dimethylaminopropyl) carbodiimide (EDC) and allowed to react overnight at 4 °C with rotation. After coupling, unreacted groups were inactivated with 0.1 M EDC, 1 M ethanolamine in 50% DMF/EtOH for 1 h at room temperature. Subsequently, beads were washed with 50% DMF/EtOH and alternating washes of 0.1 M Tris-HCl, pH 8.3 with 500 mM NaCl and 0.1 M acetate, pH 4.0 with 500 mM NaCl. Individual kinobeads were mixed in equal volumes to form the 9KiP reagent, which was stored in 20% ethanol at 4 °C in the dark until use.

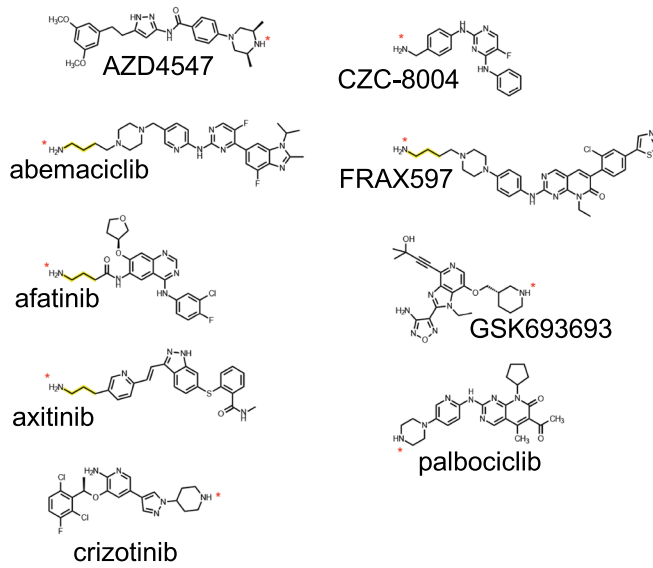
#### **Kinase enrichment by kinobeads precipitation (KiP)**

For each KiP pulldown, 20–200 µg of lysates were mixed with 10 µL of kinobeads that have been previously equilibrated in lysis buffer for 1 h at 4 °C with rotation. Kinobeads and its bound proteins were pulled down by centrifugation at 600×g for 30 s, the supernatant containing unbound proteins were aspirated. The beads were briefly washed with then successively washed two-times with 400 µL buffer containing 50 mM HEPES (pH 7.5), 600 mM NaCl, 1 mM EDTA, 1 mM EGTA with 0.5% Triton X-100 and twice the same buffer without Triton X-100 followed by two washes with MS-grade water. After the final centrifugation, all the excess liquid was aspirated off and resuspended in 30 µL of 100 mM NH<sub>4</sub>HCO<sub>3</sub> and heated at 65 °C for 10 min. 2.5 µg of trypsin was then directly added to the beads and bicarbonate mixture and digested overnight at 37 °C. To

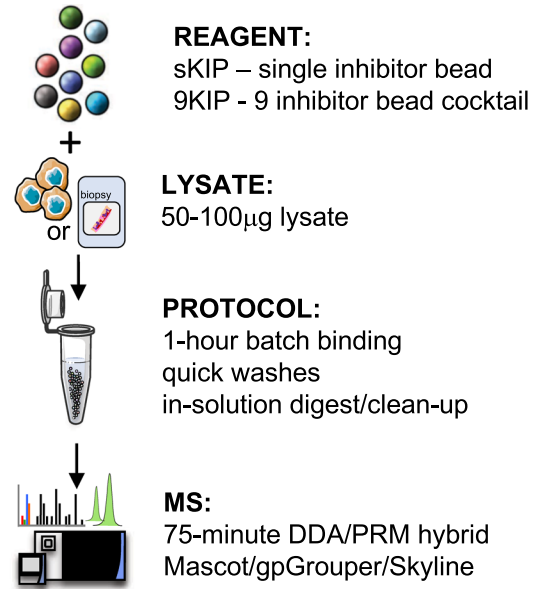
(See figure on next page.)

**Fig. 1** The kinase inhibitor pulldown assay. **A** Structure of 9 Kinase inhibitors used for KiP. For afatinib, axitinib, AZD4547, and FRAX597, a C3 Linker (yellow line) is added for conjugation. The amine group for conjugation is marked with an asterisk (\*). **B** Workflow for the kinase inhibitor pulldown assay. Native protein lysates are incubated with kinase inhibitor-conjugated beads for 1 h, and non-specific bound proteins are washed with high salt containing buffers. Inhibitor-bound kinases are digested with trypsin overnight, and digested peptides are cleaned with a detergent-removal kit and analyzed by mass spectrometry using a hybrid DDA/PRM mode. **C** Clustering of protein kinases enriched by individual inhibitors. Single inhibitor bead pulldown was carried out in triplicates for the 6 reference cell line mixture (6REF). Hierarchical clustering analysis of kinases in these experiments clearly shows that each kinase inhibitor pulls down distinct pools of kinases. Kinase classification by illuminating the Druggable Genome (IDG) Target Development Level (IDG-TDL) is indicated with different colors [26]. Green: Tbio, orange: Tchem, blue: Tclin, black: Tdark. FunCats are an in-house annotation of Functional Categories for different kinase targets including lipids (KI-L), metabolite (small molecule) (KI-M), proteins (KI-P) and unknown (KI-X). FunCats mapping can be found in the Additional file 2. **D** The Kinome tree with identified kinases highlighted. Colors represent IDG TDL classifications, and the size of the circle represents number of inhibitors that can pull down that kinase. Image rendered with KinomeRender [25]. Green: Tbio, orange: Tchem, blue: Tclin, black: Tdark. Original kinome tree illustration reproduced courtesy of Cell Signaling Technology, Inc. ([www.cellsignal.com](http://www.cellsignal.com))

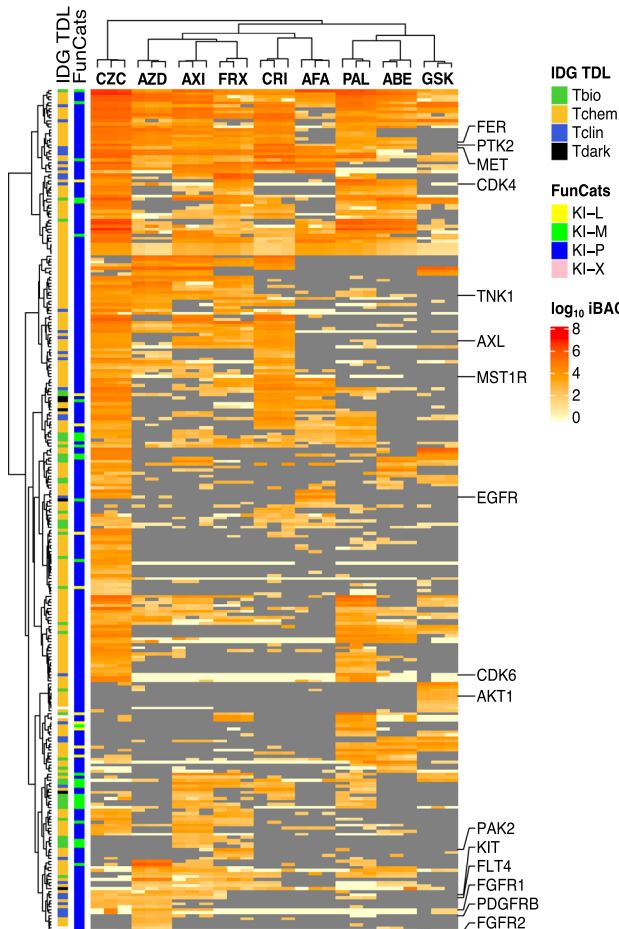
**A.**



**B.**



**C.**



**D.**

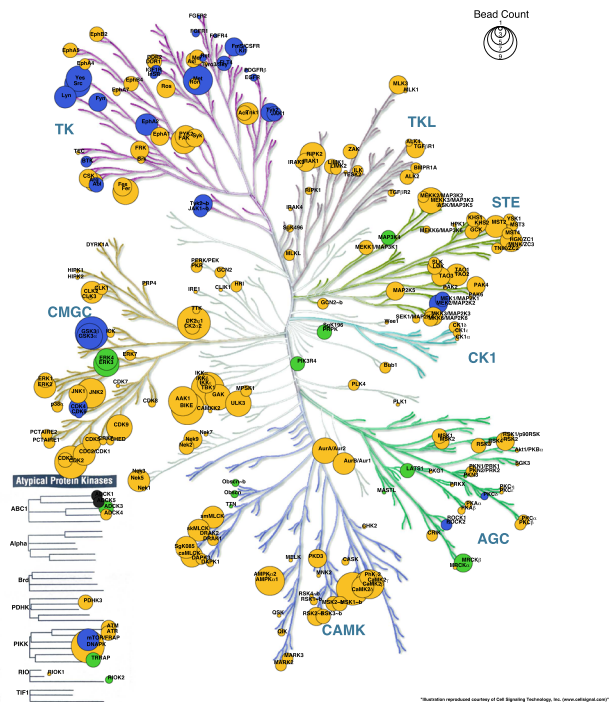


**Fig. 1** (See legend on previous page.)



remove the remaining detergent prior to MS analysis, the digested peptide mixture was processed using the HiPPR Detergent Removal Kit (Thermo) according to manufacturer's directions and dried by speed-vac prior to MS analysis.

### Mass spectrometry

#### Acquisition settings

Digested peptides were analyzed by Orbitrap Fusion Lumos mass spectrometer coupled with EASY-nLC™ 1200 system (Thermo Fisher Scientific) for all DDA, PRM, and hybrid (both DDA and PRM) methods. One fourth of peptides from KiP was loaded to a trap column (150  $\mu\text{m} \times 2$  cm, particle size 1.9  $\mu\text{m}$ ) with a max pressure of 280 bar using Solvent A (0.1% formic acid in water), then separated on a silica microcolumn (150  $\mu\text{m} \times 5$  cm, particle size, 1.9  $\mu\text{m}$ ) with a gradient of 5–28% mobile phase B (90% acetonitrile and 0.1% formic acid) at a flow rate of 750 nL/min for 75 min. For DDA scan, a precursor scan was performed in the Orbitrap by scanning m/z 300–1200 with a resolution of 120,000 at 200 m/z. The 20 most intense ions were isolated by Quadrupole with a 2 m/z window and fragmented by higher energy collisional dissociation (HCD) with normalized collision energy of 32% and detected by ion trap with rapid scan rate. Automatic gain control targets were  $5 \times 10^5$  ions with a maximum injection time of 50 ms for precursor scans and  $10^4$  with a maximum injection time of 50 ms for MS2 scans. Dynamic exclusion time was 20 s ( $\pm 7$  ppm). For PRM scan, pre-selected peptides were isolated by quadrupole followed by higher energy collisional dissociation (HCD) with normalized collision energy of 30% and product ions (MS2) were scanned by Orbitrap with a resolution of 30,000. Scan windows were set to 4 min for each peptide.

#### Raw data processing

DDA data processing largely follows that reported previously [18]. Briefly, Proteome Discoverer (PD version 2.1; Thermo Fisher Scientific) was used for peak area detection and to facilitate database search using the Mascot search engine (2.5.1, Matrix Science, London, UK) [19]. PSM validation was performed with Percolator [20] and filtered to 5% FDR, and rolled up to gene products with gpGrouper [18].

For relative quantification of PRM data, raw spectrum files were searched with Mascot, and resulting mgf output was imported to Skyline with raw spectra. Up to six strongest product ions were used to calculate peptide area. To ensure accurate quantification, all AUC ranges were manually adjusted in Skyline (version 21.2.0.425) [21]. During manual examination, any of the top six most intense peaks that did not have good alignment and

similar peak shape to other fragment ions and the precursor ion were excluded. The sum of the area of product ions for each peptide was used to quantify each protein. Protein levels were median normalized and log transformed before further analysis.

### Peptide synthesis

Peptides were purchased from Thermo Scientific Custom Peptide synthesis service and Vivitide. The peptides were purified to >95% purity by HPLC. Peptide mass was confirmed by mass spectral analysis and original concentration/net peptide content were determined by amino acid analysis. The peptides were dissolved in 20% acetonitrile/water and stored at  $-80$  °C. A heavy peptide mixture stock was prepared by mixing an equimolar amount of each peptide with the concentration at 1  $\mu\text{M}$  or 100 nM in 20% acetonitrile and 0.1% formic acid and it was diluted 10 times to make the final peptide mixture. Final peptide mixture was aliquoted to avoid multiple freeze/thaw and stored at  $-80$  °C until use.

### SureQuant

All SureQuant analysis was performed with Orbitrap Exploris 480 mass spectrometer (Thermo Scientific) coupled with Evosep One liquid chromatography system. Peptides were separated with 8 cm C18 column (EV-1109) using 30 samples per day method from Evosep One (44 min gradient).

### Survey MS analysis

Mixture of heavy peptides were separated with 8 cm C18 column (EV1109) using 30 samples per day method and the Exploris was operated in data dependent acquisition (DDA) mode with an inclusion list. Full scan spectra (300–1500 m/z, 120000 resolution) were detected by the orbitrap analyzer with automatic gain control targets of 300% and maximum injection time of 50 ms. For every full scan, up to 70 ions were subsequently isolated if the m/z was within  $\pm 10$  ppm of targets on the inclusion list and reached an intensity threshold of  $1e^5$ . Ions were collected with a maximum injection time of 10 ms, normalized AGC target 1000% and fragmented by HDC with collision energy 27% and detected with 150–1700 m/z and resolution 7500.

### SureQuant analysis

Custom SureQuant acquisition template was built according to Thermo's guidance and previously described method [22]. Full scan spectra were collected with 300–1500 m/z, AGC target 300%, maximum IT

50 ms, resolution 120,000. Peptide matching the  $m/z$  within  $\pm 3$  ppm on the inclusion list were isolated (isolation window 1  $m/z$ ), fragmented (HCD collision energy 27%) and detected (150–1700  $m/z$ , resolution 7500, AGC target 1000%, maximum IT 10 ms). A product ion trigger filter next performs pseudo-spectral matching, only triggering a MS2 event of the endogenous, target peptide at the defined mass offset if  $n \geq 4$  product ions are detected from the defined list. When triggered, light peptide MS2 scan was performed as follows: resolution 60000, 150–1700  $m/z$ , AGC target 1000%, maximum IT 116 ms. Sample measurements were normalized to the total ion chromatogram as a proxy for total peptide input after enrichment by KiP.

### Statistical analysis

In addition to KiP PRM data generated herein, three additional datasets were used to examine druggable kinases that are differential between basal and luminal tumors within and across methods.

RNAseq data was accessed as described previously [23]. The dbGAP accession number phs000611 ([http://www.ncbi.nlm.nih.gov/projects/gap/cgi-bin/study.cgi?study\\_id=phs000611.v1.p1](http://www.ncbi.nlm.nih.gov/projects/gap/cgi-bin/study.cgi?study_id=phs000611.v1.p1)) while full proteome profiling and phosphosite expression data were downloaded from [24]. WHIMs 02, 04, 06, 08, 09, 11, 12, 13, 14, 16, 18, 20, 21, 24, 25, 27, 30, 35, and 43 were used from the proteomics data; WHIMs 09, 37, and 47 were excluded as it was determined that a different pooled reference control was used for these samples. WHIM 17 and 46 were also excluded as they subsequently proved to be EBV-associated lymphoproliferative lesions. RNAseq data analysis included all available WHIM data, including WHIM 03, 05, 22, 26, 37, and 47, again excluding the EBV-associated WHIMs 17 and 46. Both proteomics datasets were filtered for observations in at least 10 samples and mapped to the gene level. The phosphosite data was rolled up into a single value by averaging all phosphosites per gene as an estimate of the relative phosphorylation status of each protein. RNASeq TPM expression data was log transformed and converted into ratios based on the median value per gene.

For differential expression of druggable kinases between basal and luminal breast tumors, a Student's *t*-test was performed for each gene across each dataset (KiP PRM, Profiling, Phosphoprofiling, and RNA). Resulting *p* values were corrected for multiple hypothesis testing with the Benjamini–Hochberg procedure.

## Results

### A combination of single-drug kinase inhibitors efficiently enriches the kinome

Nine different inhibitors (9KiP) were selected to maximize the coverage of kinases relevant for breast cancer: Palbociclib (CDK4/6 inhibitor), Crizotinib (*c*-MET and AXL inhibitor), CZC-8004 (non-specific tyrosine kinase inhibitor), Axitinib (VEGFR and PDGFR inhibitor), GSK690693 (AKT inhibitor), AZD4547 (FGFR and VEGF inhibitor), Afatinib (EGFR and ERBB2 inhibitor), Abemaciclib (CDK4/6 inhibitor), and FRAX597 (PAK inhibitor) (Fig. 1A). Kinobeads were synthesized by coupling kinase inhibitors to ECH-Sepharose beads via an amide bond (-C-N-). For this coupling reaction, the kinase inhibitor must contain a primary or secondary reactive amine (-NH<sub>2</sub> and -NH-, respectively) that can be covalently linked to the carboxyl group of the ECH-sepharose beads using EDC (1-ethyl-3-(3-dimethylaminopropyl)carbodiimide hydrochloride) as the reactive intermediate. As Afatinib, Abemaciclib, FRAX597 and Axitinib do not have the necessary amine reactive group, we modified these drugs to add a reactive group by adding a short C3 linker, taking care to avoid disrupting the drug-kinase binding pocket (demonstrated with Abemaciclib in Additional file 1: Figure S1A). In the case of Afatinib, an irreversible inhibitor of EGFR, we made an additional modification where the ethylene bond that reacts with Cys797 of EGFR was changed to an ethane bond, no longer making its inhibition irreversible. Removing the reactive ethylene bond on Afatinib derivative increases the ability of this drug to capture EGFR family members, including HER2, and other RTKs.

We aimed to establish a microscaled kinase enrichment protocol that can ultimately be applied to diagnostic samples with limited material such as frozen tumor biopsies. There are two general approaches to enriching the kinome on immobilized inhibitor beads: large-scale column-based MIB (Multiplexed Kinase Inhibitor Beads) protocols that require milligram input scales and unpacked “batch” bead pull-downs such as those used by Kuster's laboratory in 500  $\mu$ g scale. Since biopsies offer 20–100  $\mu$ g of protein for native protein lysates and clinical applications demand fast turnaround, we have focused exclusively on evaluating low input protocols. Our microscale KiP protocol substantially lowers the sample requirements for protein lysates to sub 50  $\mu$ g levels and can be completed in 2 days (Fig. 1B).

### Characterization of single-drug kinase inhibitor pulldown beads (sKiPs) for kinome enrichment

To evaluate the immobilized inhibitors in capturing intended target kinases and additional off-target polypharmacology, we tested each individual kinobead-inhibitor using cell lysates. A distinct spectrum of kinases was identified with each kinobead (Fig. 1C). Because no individual cell type expresses every kinase in the genome, we used published RNA sequence data to identify six cell lines (6Ref) that together express a comprehensive array of protein kinases. Using 100  $\mu$ g of 6Ref lysate, each kinobead pulldown was performed in technical triplicates. The measured kinome has a high degree of technical reproducibility within each kinobead, with Pearson R values exceeding 0.9 (Additional file 1: Figure S1B). Furthermore, the often disparate expression values across different kinase affinity beads underscores the contribution of multiplexing drugs to maximum kinome enrichment. For the eight substrate-specific kinase inhibitors (excluding the pan tyrosine kinase inhibitor CZC-8004), each were found to capture one or more of their intended targets, with exception of ERBB2, likely due to low levels of expression. ERBB2 capture was later confirmed by adding the ERBB2-overexpressing BT-474 cell line to form the 7Ref mix, which was used in all subsequent protocol optimization and quality control experiments. In addition to protein kinases focused on in this study, we also detected significant number of metabolite and lipid kinases, attributed to the conservation of the ATP-binding domain. For the purposes of this study, we remain focused on protein kinases.

The kinobeads collectively cover a large spectrum of the human kinome, as visualized by KinomeRender [25] (Fig. 1D). In addition to tyrosine kinase (TK) and tyrosine kinase-like (TKL) families, which are direct inhibitor targets, we observed kinases across all other families including Casein Kinase 1 (CK1) family, the serine/threonine kinase STE family, CMGC, AGC, Calmodulin/Calcium regulated kinases (CAMK), and some members of the Atypical Protein Kinase family. All kinobeads enrich kinases across more than one family (Additional file 1: Figure S1B). While many kinases are overlapping between multiple kinobeads, each kinobead has a unique subset of kinases it can enrich (Additional file 1: Figure S1C). Importantly, most of the targetable kinases with a clinically approved drug (T-clin) or with a pre-clinical tool compound (T-chem) by the NIH Illuminating the Druggable Genome (IDG) Consortium [26], are well represented. This highlights the potential of our kinome profiling approach to uncover unexpected therapeutic avenues where immediate application or repurposing can be indicated based on clinical sample profiling.

### Microscaled KiP effectively enriches the kinome

We performed kinome pulldowns across a range of protein input amounts to further investigate the feasibility of microscaling using the 9KiP reagent and the 7Ref lysate. For assessment of assay linearity in low-microscale samples, 10  $\mu$ L 9KiP beads were used with increasing amounts of 7Ref lysate (0, 12.5, 25, 50, 100, and 200  $\mu$ g) (Fig. 2A). More than 220 kinases were identified at the lowest level of 12.5  $\mu$ g lysate, increasing to ~300 kinases with 50  $\mu$ g of input (Fig. 2B). Increasing input did not further increase the number of kinases observed, but the total quantity (based on MS1 AUC) of kinases detected increased linearly (Additional file 1: Figure S2A). 50  $\mu$ g of protein lysate is sufficient input for the MS-based detection of the expressed kinome after KiP enrichment. The total amount of bound kinases, evaluated here as total iBAQ value, scaled linearly across all levels of input, suggesting that 10  $\mu$ L of the 9KiP cocktail is not saturated using up to 200  $\mu$ g of lysate, and the KiP assay has a good linear range for kinome recovery for low microgram protein samples. The linear relationship to protein input holds true for most identified kinases, including ERBB2 (Additional file 1: Figure S2A). Quantification of some highly abundant kinases, including CDK4 and PRKDC, begins to saturate at 50  $\mu$ g lysate (Additional file 1: Figure S2B–E). These data underscore the importance of characterizing individual kinase response curves should accurate quantification be needed in more stringent clinical setting. Full data available in the Additional file 2.

To determine the binding percentage and capacity of KiP, pulldowns were repeated with supernatants containing unbound proteins from preceding KiP enrichments (Fig. 2A). 10  $\mu$ L of 9KiP beads were used with 50  $\mu$ g and 100  $\mu$ g amounts of 7Ref lysate, and their supernatants were subjected to two subsequent rounds of KiP enrichment with new beads. In each round, kinases decrease modestly by number of identifications but dramatically by level (Fig. 2C). With 50  $\mu$ g of lysate, 84% of kinases are identified after the first depletion, and 59% of kinases after the second. The first depletion input recovers 28% of the original kinase abundance, and the second depletion less than 10%. These trends were similar for 100  $\mu$ g, however more kinases were observed overall as total levels were higher than those observed for 50  $\mu$ g. The total kinases observed, linear range and binding percentage are sufficient to reliably utilize the pulldown to quantify kinases. The data dependent acquisition schemes utilized for these experiments are stochastically less quantitative for lower abundance kinases. Full data is available in the Additional file 2.

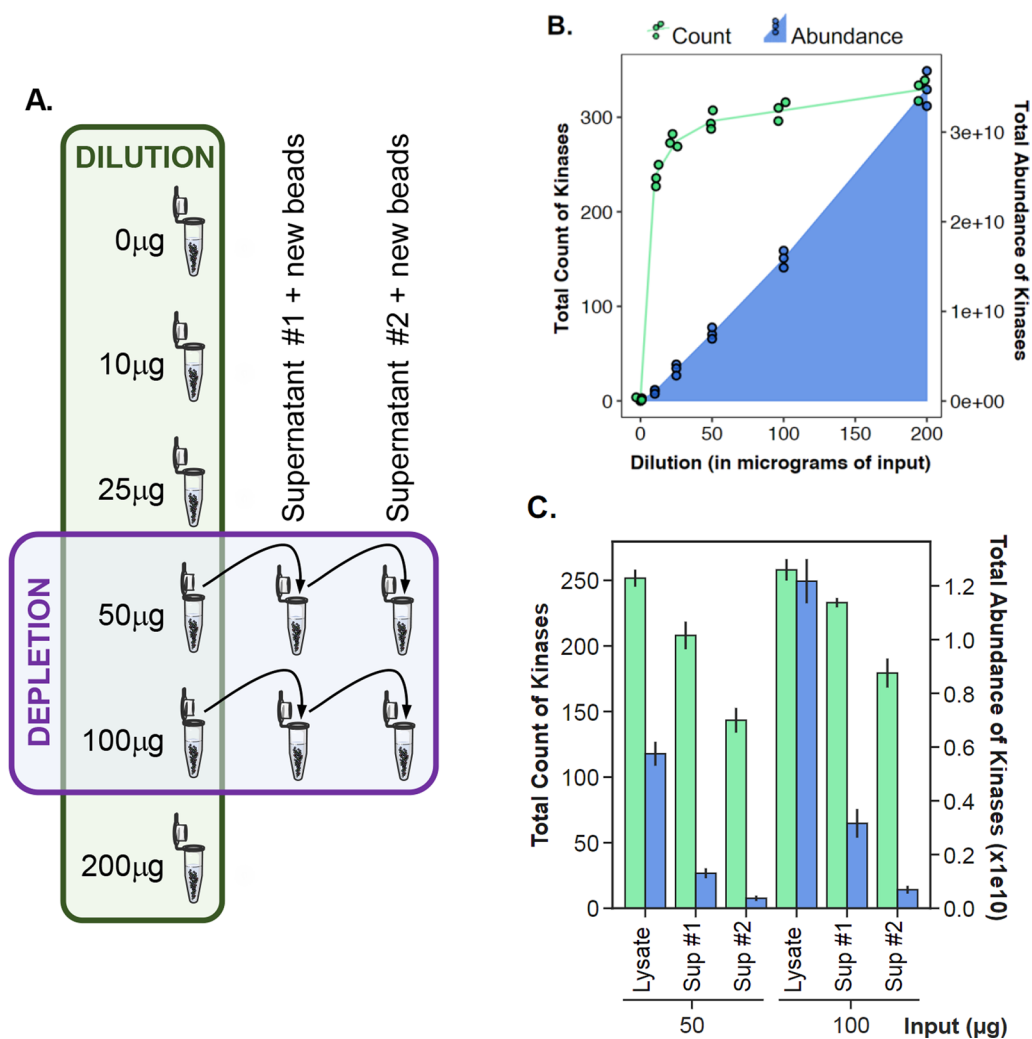


**Fig. 2** Linearity and binding efficiency of KiP. **A** Schematic for KiP with different input amounts and serial depletion. KiP was performed with increasing amounts of 7REF lysate. For the depletion experiments, KiP was repeated twice with the supernatant from 50 to 100 μg KiP experiments. **B** Number of kinases identified and kinase abundance from different input experiments. Kinase numbers are plotted in green and abundance is plotted in blue. **C** Number of kinases identified and kinase abundance from depletion experiments. Kinase numbers are plotted in green and abundance is plotted in blue

### PRM assay development and parameters

To increase quantitative metrics, we optimized a parallel reaction monitoring (PRM) assay with targets identified in our pulldown assays. We identified 55 druggable kinases picked based on data available from the Cancer Therapy Evaluation Program (CTEP) and previous literature [27], and identified an additional 47 kinases suggested to be differentially expressed between basal and luminal subtypes in our previous profiling experiments of breast cancer patient derived xenograft models (data not shown). To improve the sensitivity, accuracy, and precision of the assay, we designed PRM assays with representative peptides. Initially, five to seven peptides were chosen empirically based on their performance in

a collection of all (>7000) experiments from our laboratories (Additional file 1: Figure S3A). We deprioritized peptides that either have a low Mascot Ion Score (<20), are observed to be post-translationally modified for more than 10% of all PSMs, contain a tryptic missed cleavage event, are a product of a larger peptide with tryptic missed cleavages, or if the sequence is shared across multiple gene products. Due to our work murine PDX models, we further deprioritized peptides shared across human and mouse. When possible, we used peptides representative of all gene-specific protein isoforms. After narrowing down to 2–4 peptides per gene product, we evaluated best responders by testing for linear responses of these peptides on dilutions of the same KiP lysate. Ideal



candidates had narrow and approximately symmetrical peaks, intensity scaling proportionally to the amount of input material, and do not contain non-specific interfering peaks. And identified 2–4 peptides by best response curve and peptide peak shapes (Additional file 1: Figure S3B). Full lists of all druggable and other kinases of interest, as well as peptides we characterized for PRM, are available in the Additional file 2.

Kinases are quantified by PRM with equal or greater precision than when quantified by DDA. KiP experiments for 6Ref lysate were performed across 4 different concentrations (12.5–100  $\mu\text{g}$ ) in technical duplicates, and samples were run on the mass spectrometer with a 75 min label-free hybrid DDA/PRM method

including >200 PRM targeted peptides with 5-min retention time windows. All proteins show strong correlation to input levels from PRM quantification, regardless of their relative abundance (Fig. 3A). In contrast, while DDA achieved good correlation for the most abundant kinases, measurements deteriorated for lower-level proteins. For example, both DDA and PRM show consistent quantification for ERBB2, the 16th most abundant kinase in intensity (Fig. 3B). However, the less abundant CDK6 kinase was not consistent by DDA, whereas its levels by PRM followed input levels accurately. Poor correlation for less abundant kinases by DDA is partly due to lack of peptide identification; however, Pearson correlation coefficients are stronger for PRM than DDA even

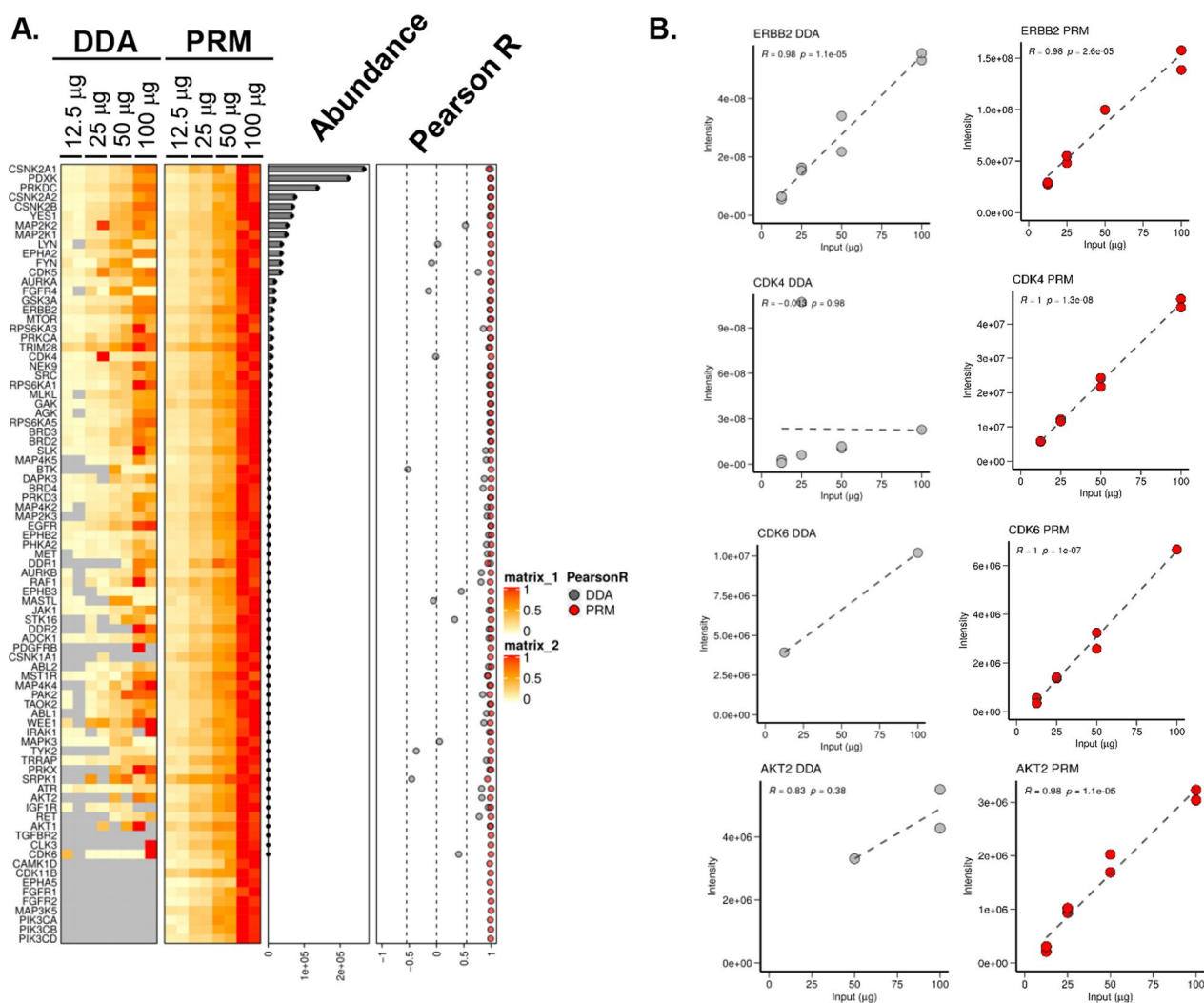


**Fig. 3** Quantification of kinases by DDA and PRM. **A** KiP experiments for 7REF cells were performed at 4 different concentrations (from 12.5  $\mu\text{g}$  to 100  $\mu\text{g}$ ), and samples were run on the mass spectrometer using hybrid mode (DDA/PRM). Although both DDA and PRM produce good correlations for many kinases, PRM dramatically improves quantification for lower abundance kinases. **B** ERBB2, CDK4, CDK6, and AKT2 quantifications are plotted as representative examples

when samples without identifications are excluded from analysis (Fig. 3B). Unsurprisingly, PRM quantification using verified peptides markedly improves quantification accuracy of enriched kinases, particularly for proteins of lower abundance. In summary, KiP-PRM yields sensitive, accurate and precise measurements of kinases. Statistical summary available in the Additional file 2.

#### PDX subtyping with KiP-PRM

KiP-PRM classifies and subtypes breast cancer xenografts in concordance with comprehensive molecular profiling. We applied KiP to 16 breast cancer xenografts previously generated and characterized by deep transcriptome, proteome, and phosphoproteome sequencing [24]. We previously demonstrated that these models are relatively stable across passages and thus are a representative set of breast cancer subtypes [18]. 50 µg of protein lysate from PDX tumors was used for KiP enrichment, and all experiments were performed in technical duplicates. One third of peptides post KiP enrichment were analyzed using a DDA/PRM hybrid method, and a total of 91 kinases were quantified by PRM. Hierarchical clustering using kinases measured by PRM separates tumors into groups corresponding primarily to basal and luminal PAM50 [28, 29] subtypes (Fig. 4). The two HER2-expressing tumors (WHIMS 8 & 35) fall into the two different main clusters, suggesting substantial kinase differences between the models. Nevertheless, both tumors have the highest expression of ERBB2 across the cohort, as expected. Lastly, the claudin-low tumor WHIM12 clusters near, but distinct from the basal subgroup. This is consistent with the consensus that claudin-low tumors can be related to basal subtypes [30] and with a recent finding that most claudin-low tumors have a basal-like intrinsic subtype [31].

To examine the statistical power of the KiP-PRM assay, we performed two-sample t-tests between the basal and luminal subtypes (grouping luminal A and B together) for all proteins that were quantified by the assay as well as for analytes from the previously published iTRAQ protein, iTRAQ phosphoprotein, and RNASeq datasets [24]. For the KiP-PRM data, we used the mean value across two technical replicates. Using the uncorrected p-value threshold of 0.05, 36 kinases are significantly

differentially expressed between PDX models in the KiP data. By the same metric, 13 Kinases are upregulated in basal models, and 23 kinases are upregulated in luminal. As expected, EGFR is enriched in basal PDXs, and known luminal BRCA associated kinases RET and IGF1R are elevated in luminal PDXs.

KiP differentially quantifies more subtype specific kinases (n=36) than iTRAQ proteome profiling (24 kinases). This additional quantification fidelity likely arises from enrichment and increased precision due to PRM targeting; most significant kinases in the KiP-PRM data have similar directionality in the proteome and phosphoproteome dataset. Further, KiP-PRM measurements correlate well across the majority of proteins with a median Pearson correlation above 0.5 for both protein-based measurements—in contrast the correlation with RNASeq which exhibits a bimodal distribution and a lower median Pearson correlation of 0.23.

RNA-sequencing identifies a similar number of subtype-specific kinases (n=35) that poorly overlap with those found to be significant in proteomic profiling or KiP. The distribution of significant kinases from the RNA-seq data is uneven with 32 being basal specific kinases while only 3 are upregulated in luminal tumors. Interestingly, when examining all proteins identified through KiP-DDA, many RNA related proteins appear upregulated in basal BRCA. These results are consistent with previous comparisons between RNA and protein expression levels [32]. While there is substantial overlap with previous data with regard to subtype-specific proteins, KiP PRM highlights additional kinases that differ between subtypes not necessarily exhibited from previous omics analyses. This highlights the benefits the enrichment and precise quantification afforded by KiP-PRM. PRM measurement data is available in the Additional file 2.

#### Patient sample subtyping with KiP-PRM

Given the subtyping of PDX tumors achieved using KiP, we pursued the analysis of clinical samples obtained from previously studied cohorts: Luminal subtype from Preoperative Letrozole (POL) clinical trial [33], and ERBB2+ samples from the Discovery protocol 1 (DP1; NCT01850628) study, on which we have previously

(See figure on next page.)

**Fig. 4** KiP classifies 16 WHIM PDX tumors according to their intrinsic subtype. Kinases from 16 breast cancer xenografts were enriched by KiP, and druggable kinases and subtype-specific kinases were quantified by PRM. 50 µg of protein from PDX tumors was used, and all experiments were performed in duplicates. Clustering analysis of kinases distinguishes basal subtype samples from luminal subtype samples, and claudin-low samples are separated from all other samples. A basal specific kinase, EGFR is enriched in basal PDXs, and luminal specific kinases, RET and IGF1R, are enriched in luminal PDXs. KiP is able to capture most of subtype-specific kinases identified in previous RNA-sequencing or proteome profiling studies [24]

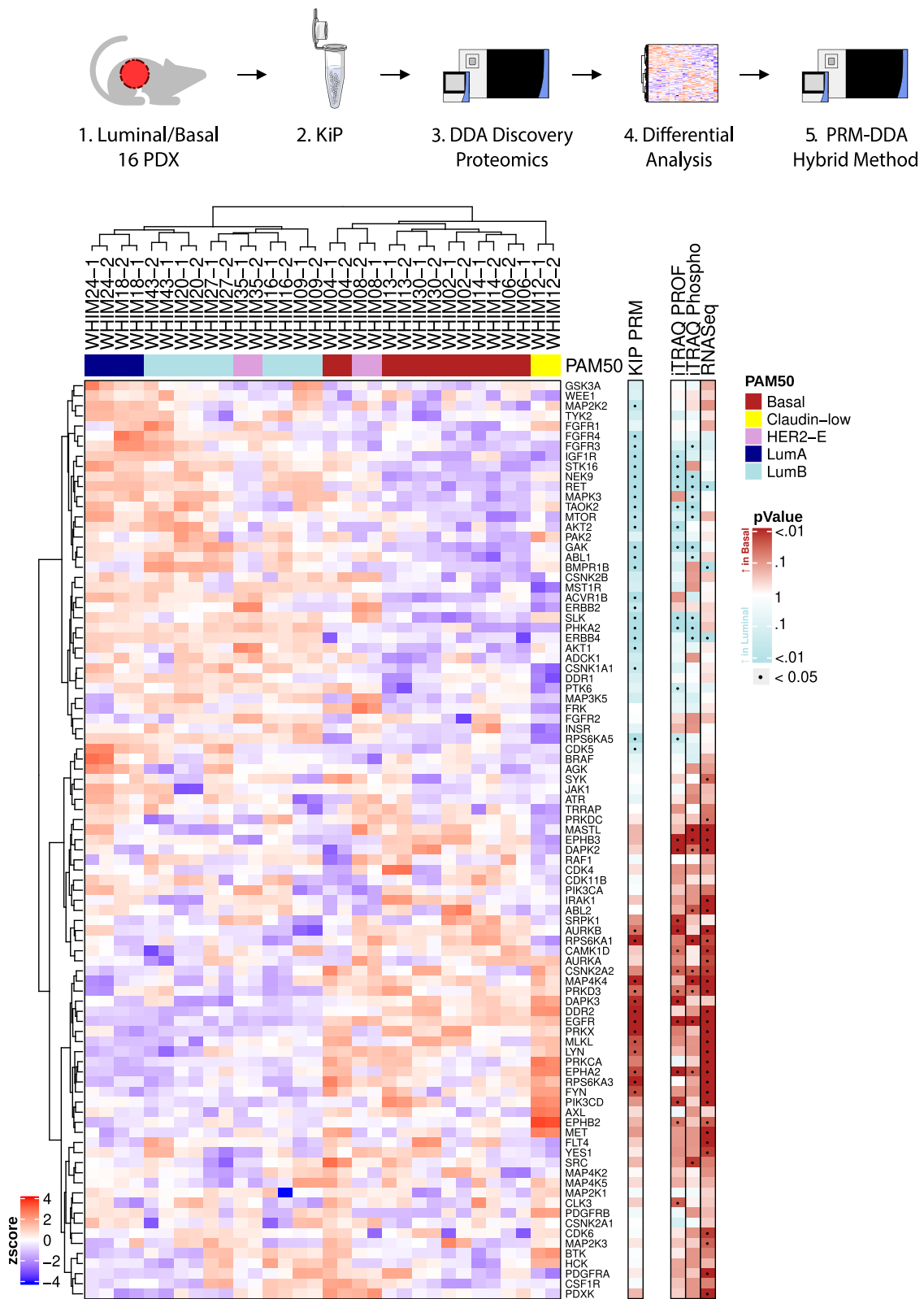


Fig. 4 (See legend on previous page.)

reported [34]. We used the BioText protocol [34] for sample processing. Approximately 50–100 µg of lysate obtained from OCT-frozen blocks was used for each enrichment, and one-third to one-half of the post-enrichment protein pool was used for analysis. The majority of samples analyzed have previous RNAseq results, from which stromal scores, immune scores and their combination: Cibersort, xCell and ESTIMATE scores were derived [35, 36]. These metrics inform of the quality and purity of the tumor sample and the microenvironment of the tumor. In total, 16 luminal and 21 ERBB2+(HER2) samples were analyzed (Fig. 5). K-means clustering of the samples yielded 3 subgroups: one Luminal and two HER2 groups. Resistant and sensitive samples tend to group together within subtypes, and ESTIMATE scores were highest in HER2 cluster 3.

HER2 is significantly elevated in the HER2 cohort ( $p$ -value =  $8E-10$  Welch's  $t$ -test) with a 53.89-fold change as compared to the luminal cohort. DDR2, FGFR1, JAK3, MAP4K4 and CSNK2A1 are also elevated in the HER2 cohort, with DDR2 being the best delineator of the two subtypes with a  $p$ -value of  $7E-18$  and 188.64 fold change versus luminal. Conversely, CDK4, CDK5 and PIK3CA were significantly elevated in the Luminal cohort ( $p$ -value  $< 1E-6$  Welch's  $t$ -test). These findings are consistent with previous ER+ and HER2+ breast cancer studies and our observations with PDX models. In summary KiP-PRM is able to separate breast cancer patient samples into clinical subtypes using 100 µg of lysate or less.

### IS-PRM subtyping with KiP

Encouraged by the effective subtyping of patient samples with KiP, we decided to pursue a clinically applicable absolute quantification approach. To maximize clinical efficacy of our KiP approach, we developed an Internal Standard Triggered-Parallel Reaction Monitoring (IS-PRM) assay using 106 heavy peptides identified from our PRM studies. We removed the hybrid component of the PRM method and shortened the gradient to 44 min, resulting in throughput of 30 injections a day. Lysates used in the previous PDX-PRM analysis were combined with either 10 fmol (98 peptides) or 100 fmol (8 peptides) of stable isotope labeled peptides. All results were manually validated using Skyline. Quantified values available in Additional file 2. To establish the quantitative parameters

of this approach, we ran a mixture of Luminal PDX samples in 18 replicates. We achieved an average coefficient of variance (CV) of 9.28% (2.2–27.2%) for 80 peptides (Additional file 1: Figure S3). IS-PRM KiP recapitulates the clustering observed in the KiP-PRM data. Luminal and basal PDX models cluster together (Fig. 6). Further, Luminal A, Luminal B and HER2 subtypes clustering is comparable with that observed in the PRM dataset. The list of characterized peptides and the PRM and SureQuant measurements are both available in the Additional file 2.

### Discussion

The kinase inhibitor pulldown assay is a robust, reproducible and clinically relevant approach to successfully enrich and quantify the majority of the kinome. The current inhibitor combination used in our pulldown yielded over 300 distinct kinases, and it is likely that additional kinases of interest can be identified through further assay development. Should a novel inhibitor target a kinase that is not binding to the current KiP assay, that novel inhibitor may be immobilized and added as an additional component to the matrix. During the development of this method, we attempted multiple different inhibitor combinations and found no detriment to identification capacity with additional inhibitors. Thus, KiP is modular and additional inhibitors may be added. This capability may even extend beyond kinase inhibitors to other drug classes in order to quantify additional low-abundance and biologically relevant targets.

While the patient sets are from vastly different cohorts, and thus expected to have analytical differences, KiP identified kinases with an extreme dynamic range afforded by relatively clean, and abundant spectra due to enrichment. This is most obvious in the IS-PRM dataset where subtype defining kinases are orders of magnitude differentially expressed between samples. In contrast, isobaric labeling approaches did not as robustly identify kinases that are differentially expressed when compared to PRM. With the experimental design of this study, it is impossible to know what the 'base truth' is for differences in kinase expression between samples, and thus KiP may have yielded false positives. However, given the well-established phenotypic and pathological differences

(See figure on next page.)

**Fig. 5** KiP clusters breast cancer patient samples by subtype by quantifying kinases. KiP-PRM clusters breast cancer patient samples by intrinsic subtype, identifies subgroups within subtypes, and partially clusters resistant patients within subtype. 37 patient samples from a HER2+ cohort and a luminal cohort were processed with the KiP assay and analyzed by PRM. HER2 is highly enriched in the HER2+ cohort, and luminal associated kinases such as CDK4 were elevated in the Luminal cohort. *ypCR* yes pathological complete response, *LowerProlif* Lower Proliferation, not a complete response, *CS Absolute Score* CIBERSORT ABSOLUTE Score



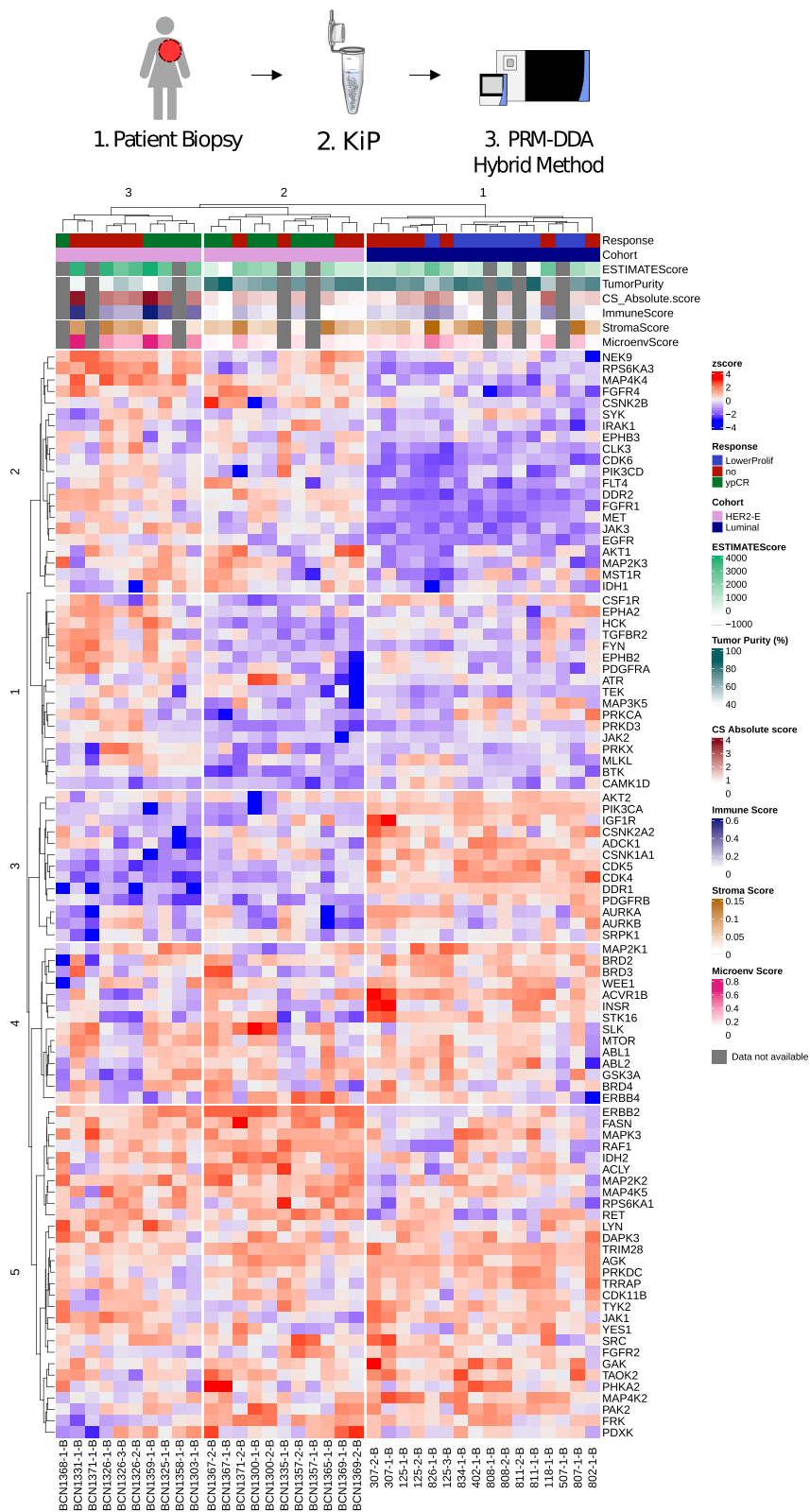
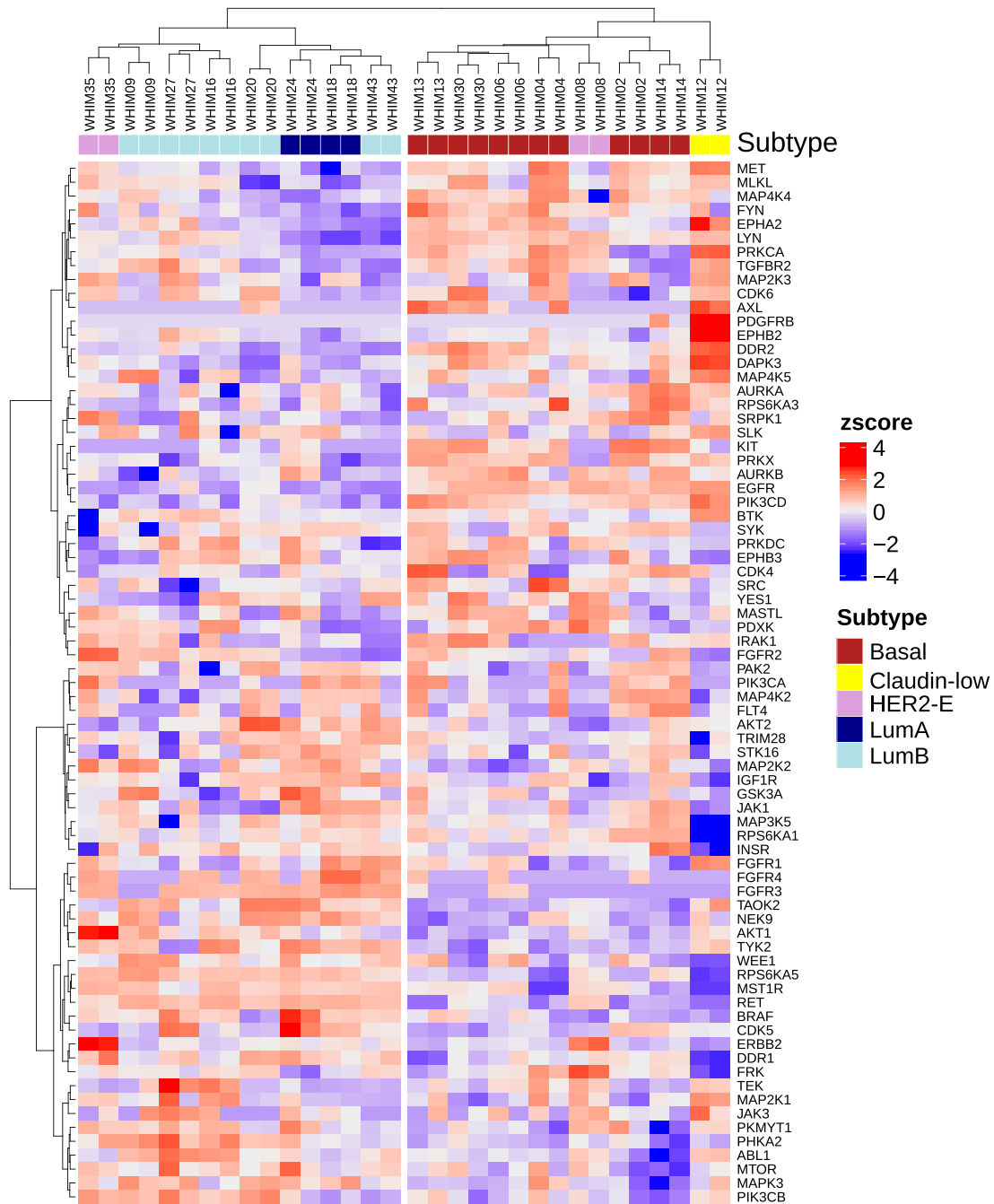
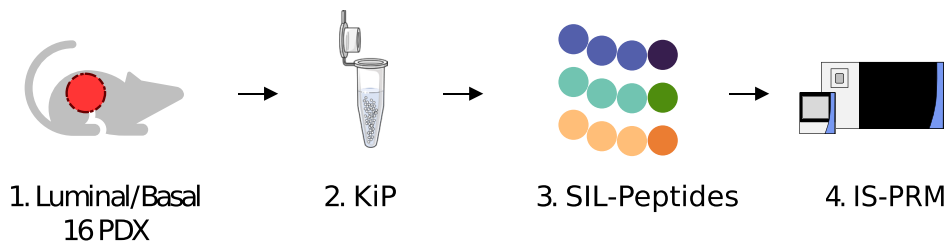


Fig. 5 (See legend on previous page.)



**Fig. 6** Prototype clinical implementation with IS-PRM for 16 PDX KiP samples. Heavy isotope labeled triggered acquisition of KiP enriched kinases in combination with an Evosep and Exploris 480 as a prototype clinical assay. Nearly identical clustering observed in the PRM method was obtained

between luminal and basal breast cancer, there is potential utility in any differentially identified target.

In this study Orbitrap instruments, DDA and PRM/IS-PRM were exclusively used with KiP. The benefits of KiP enrichment are independent of the type of mass spectrometer employed, and other available platforms with triple quadrupole and time-of-flight detectors will also have empirically improved quantification of kinases. Additionally, data independent acquisition techniques will similarly benefit as spectra will inherently be less convoluted. Similar benefits are observed with antibody-based enrichment strategies (such as immuno-MRM [37]). This study serves as a prototype affinity assay that is not antibody based. This has the major advantage of not requiring a specific and validated antibody, which often requires significant effort to develop. In addition, the ability to acquire both DDA and PRM data in a single run allows for further unbiased exploration of proteins not limited to those targeted for PRM. While PRM acquisition takes precedence over DDA and thus reduces the quality of this discovery dataset, this is a minor compromise that is made up for by the additional data we can acquire on potentially minute sample quantities. This hybrid method ensures the proteins of particular interest are measured with the high accuracy and precision afforded by the PRM method, while also providing an unbiased survey of the full peptide pool.

A major challenge in the clinical implementation of KiP is the need for native lysate. Effective binding of kinases to inhibitors required kinases to not be denatured or cross-linked. Current methods of extracting proteins from FFPE blocks use heat, xylene and/or detergents. These methods are not compatible with KiP. Flash frozen and OCT-embedded samples are viable alternatives, but widespread adoption of MS compatible sample preservation and storage is still obligatory. Clinical protocols that incorporate procedures that preserve the bioactivity of the proteome are uncommon, but certainly feasible, as our study demonstrates. As more clinical trials consider better sample preservation methodologies, the availability of larger cohorts with native lysates will allow for further bioactive proteome profiling approaches such as KiP.

## Supplementary Information

The online version contains supplementary material available at <https://doi.org/10.1186/s12014-023-09448-3>.

**Additional file 1: Figure S1.** KiP with single inhibitor beads (sKiP). **(A)** Cartoon render of Abemaciclib in the binding pocket of target CDK4. Original RCSB PDB number 7SJ3, [39]. Note the cyclin was removed for this render. **(B)** Correlation matrix of the resultant kinome from each sKiP (single KiP) shows technical reproducibility of each sKiP (single KiP) across 3 different technicians. **(C)** Kinase family identified by sKiP. **(D)** Kinome Tree by sKiP. Illustration reproduced courtesy of Cell Signaling Technology, Inc. Colors are IDG kinase classifications. Green: Tbio, orange: Tchem,

blue: Tclin, black: Tdark. ([www.cellsignal.com](http://www.cellsignal.com)). Drug abbreviations: ABE, abemaciclib; AFA, afatinib; AXI, axitinib; AZD, AZD4547; CRI, crizotinib; CZC, CZC-8004; FRX, FRAX597; PAL, palbociclib; GSK, GSK693693. **Figure S2.** KiP with different input experiment. **(A)** KiP was carried out with different amounts of lysate (Fig. 2A) and quantified kinase levels are plotted. Illuminating the Druggable Genome (IDG) Target Development Level (IDG-TDL) category indicated with different colors [26]. Green: Tbio, orange: Tchem, blue: Tclin, black: Tdark. FunCats are an in-house annotation of Functional Categories for different kinase targets including lipids (KI-L), metabolite (small molecule) (KI-M), proteins (KI-P) and unknown (KI-X). FunCats mapping table is available in the Additional file 2. **(B-E)** ABL1, ERBB2, CDK4 and PRKDC quantification was plotted as representative examples of linear and nonlinear responses. **Figure S3.** Detailed description of peptide assessment for PRM development. **(A)** Example of qPick from iSPEC database. All the information of identified peptides for each kinase in iSPEC database are presented by qPick. It includes peptide sequence, mass, gene product number for the peptide, miscleavage, PSMs for each modification, PSMs for each charge, best ion score, average retention time, etc. Peptides were ranked by experimental PSM counts, and top 3 to 6 peptides were selected for PRM runs. However, peptides are excluded if they fall into following categories and other viable candidates exist; (1) More than 10% of PSMs has modification (2) A peptide has miscleavage in it (3) Many PSMs of that peptide are part of miscleaved peptides (4) Sequence is shared with other gene product (5) bad Mascot ion score (< 20). **(B)** Representative examples of PRM peptide selection. KiP experiment was performed with different amounts of inputs and samples ran on mass spectrometry with PRM method to choose best PRM peptides. We took the following categories into consideration. (1) Peak shapes – peaks need to be symmetrical and narrow (2) response – sum of peak areas should be proportional to input level (3) interference – there should be no other non-specific peaks. We chose the peptides which meet these categories and generated the final list of PRM peptides for kinases. For example, peptide IHWDLSTER for ADCK1 has non-specific peaks around although peptide response looks good. On the other hand, peptide LTIPILYVK for GSK3A shows bad response whereas peak shape is good and there is no non-specific band. Therefore, these peptides were excluded from the final PRM peptide list.

**Additional file 2.** Comprehensive Data Compilation from Multiple Excel Spreadsheets. ExpNo\_mapping\_table Mapping identifier to raw files. 55Druggable\_Kinases List of kinases deemed "druggable" based on available information. 47basal\_luminal\_specific\_proteins List of additional kinases of interest based on preliminary experiments. sKiPs\_counts count of Strict gene products (Mascot IonScore >= 30, q-value <= 0.01) corresponding to Figure 1. FunCats\_mapping Mapping table to in-house protein Functional Categories corresponding to Figure 1. Dilutions\_9KiP\_counts Total kinase counts across dilutions (variable input) corresponding to Figure 2. Depletions\_9KiP\_counts Total kinase counts across depletions corresponding to Figure 2. Depletions\_9KiP\_individual\_DDA Individual kinase values (iBAQ log transformed) for DDA data corresponding to Figure 2. Log scale. Dilutions\_9KiP\_individual\_DDA Individual kinase values (iBAQ log transformed) for DDA data corresponding to Figures 2-3. Log scale. Dilutions\_9KiP\_individual\_PRM Individual kinase values for PRM data corresponding to Figure 3. Linear scale. WHIM\_PDX\_PRM\_Transitions\_Sum PRM measurements for WHIM PDXs corresponding to Figure 4. Linear scale. Basal\_vs\_Luminal\_pvalues Raw p-values across datasets for WHIM PDXs corresponding to Figure 4. DP1\_POL\_Clinical-Samples\_PRM\_zscore PRM data (log transformed and zscored) for clinical samples corresponding to Figure 5. Heavy\_Peptide\_summary Summary of peptides explored for use as heavy trigger peptides. WHIM\_PDX\_SureQuant\_Transitions Transition intensities for experimental peptides, linear scale. WHIM\_PDX\_SureQuant\_TransitionsTICnorm Transition intensities for experimental peptides, linear scale, after TIC normalization.

## Acknowledgements

Authors would like to acknowledge funding support CPTAC PTRC grant National Cancer Institute's Specialized Programs of Research Excellence (SPORE) (U01 CA214125), CPTAC PGDAC Award (U24 CA210954), M.J.E. received support from the CPRIT Established Investigator Award (RR140033) and is an Emeritus McNair Medical Institute Scholar at Baylor College of

Medicine. BCM Mass Spectrometry Proteomics Core is supported in part by the Dan L. Duncan Comprehensive Cancer Center Award (P30 CA125123), CPRIT Core Facility Awards (RP170005 and RP210227) and NIH High-End Instrumentation Award (S10 OD026804). Authors would like to acknowledge the intellectual contributions from Shankha Satpathy, Ph.D., Steven A. Carr, Ph.D., Bing Zhang, Ph.D., and Daniel Keri, Ph.D.

#### Author contributions

Conceptualization—ABS, DWC, MVH, BJK, AM, MJE; bead synthesis R&D and production—DWC; BJK Data generation and experimentation—ABS, DWC, MVH, BJK, PS, JW; lead data analysis—ABS, DWC, MVH, AM, BJK, MJE; data analysis and interpretation—ABS, DWC, MVH, JW, EJ, MA, BJK, MJE; manuscript editing—all authors; funding acquisition—AM, MJE.

#### Availability of data and materials

The mass spectrometry proteomics data have been deposited to the ProteomeXchange Consortium via the PRIDE [38] partner repository with the dataset identifiers PXD044655 and PXD046169. A sample mapping table with short descriptions is available in the Additional file 2.

#### Declarations

##### Ethics approval and consent to participate

A. Saltzman: None. D. Chan: None. M. Holt: None. J. Wang: None. E. Jaehnig: None. M. Anurag: None. P. Singh: None. A. Malovannaya: None. M. Ellis: None. B. Kim and P. Singh became full-time employees of AstraZeneca and Johnson & Johnson respectively after completion of this study.

##### Competing interests

The authors declare that they have no competing interests.

##### Author details

<sup>1</sup>Mass Spectrometry Proteomics Core, Advanced Technology Cores, Baylor College of Medicine, Houston, TX, USA. <sup>2</sup>Lester and Sue Smith Breast Center and Dan L. Duncan Comprehensive Cancer Center, Baylor College of Medicine, Houston, TX 77030, USA. <sup>3</sup>Department of Molecular and Cellular Biology, Baylor College of Medicine, Houston, TX 77030, USA. <sup>4</sup>Department of Biochemistry and Molecular Pharmacology, Baylor College of Medicine, Houston, TX 77030, USA. <sup>5</sup>Present Address: MD Anderson Cancer Center, Houston, TX 77030, USA. <sup>6</sup>Present Address: AstraZeneca, Gaithersburg, MD 20878, USA. <sup>7</sup>Present Address: Johnson & Johnson, Springhouse, PA, USA.

Received: 30 August 2023 Accepted: 7 December 2023

Published online: 16 January 2024

#### References

- Atwood MM, Fabbro D, Sokolov AV, Knapp S, Schiöth HB. Trends in kinase drug discovery: targets, indications and inhibitor design. *Nat Rev Drug Discov.* 2021;20(11):839–61.
- Rian B, Ruker JD, Oshe M, Alpaz T, Esta EJR, Eng IP, et al. Efficacy and safety of a specific inhibitor of the BCR-ABL tyrosine kinase in chronic myeloid leukemia. *N Engl J Med.* 2001;344(14):1031–7. <https://doi.org/10.1056/NEJM200104053441401>.
- Ardito F, Giuliani M, Perrone D, Troiano G, Muzio LL. The crucial role of protein phosphorylation in cell signaling and its use as targeted therapy (Review). *Int J Mol Med.* 2017;40(2):271–80.
- Vogel CL, Cobleigh MA, Tripathy D, Guthel JC, Harris LN, Fehrenbacher L, et al. Efficacy and safety of trastuzumab as a single agent in first-line treatment of HER2-overexpressing metastatic breast cancer. *J Clin Oncol Off J Am Soc Clin Oncol.* 2002;20(3):719–26.
- Anastas JN. Functional crosstalk between WNT signaling and Tyrosine kinase signaling in cancer. *Semin Oncol.* 2015;42(6):820–31.
- Nakayasu ES, Gritsenko M, Piehowski PD, Gao Y, Orton DJ, Schepmoes AA, et al. Tutorial: best practices and considerations for mass-spectrometry-based protein biomarker discovery and validation. *Nat Protoc.* 2021;16(8):3737–60.
- Mertins P, Tang LC, Krug K, Clark DJ, Gritsenko MA, Chen L, et al. Reproducible workflow for multiplexed deep-scale proteome and phosphoproteome analysis of tumor tissues by liquid chromatography-mass spectrometry. *Nat Protoc.* 2018;13(7):1632–61.
- Knockaert M, Gray N, Damiens E, Chang YT, Grellier P, Grant K, et al. Intracellular targets of cyclin-dependent kinase inhibitors: identification by affinity chromatography using immobilised inhibitors. *Chem Biol.* 2000;7(6):411–22.
- Daub H, Olsen JV, Bairlein M, Gnäd F, Oppermann FS, Körner R, et al. Kinase-selective enrichment enables quantitative phosphoproteomics of the kinome across the cell cycle. *Mol Cell.* 2008;31(3):438–48.
- Duncan JS, Whittle MC, Nakamura K, Abell AN, Midland AA, Zawistowski JS, et al. Dynamic reprogramming of the kinome in Response to targeted MEK inhibition in triple-negative breast cancer. *Cell.* 2012;149(2):307–21.
- Kuhn E, Carr SA. Multiplexed immunoaffinity enrichment of peptides with anti-peptide antibodies and quantification by stable isotope dilution multiple reaction monitoring mass spectrometry. *Methods Mol Biol Clifton NJ.* 2016;1410:135–67.
- Médard G, Pachi F, Ruprecht B, Klaeger S, Heinzlmeir S, Helm D, et al. Optimized chemical proteomics assay for kinase inhibitor profiling. *J Proteome Res.* 2015;14(3):1574–86.
- Klaeger S, Heinzlmeir S, Wilhelm M, Polzer H, Vick B, Koenig PA, et al. The target landscape of clinical kinase drugs. *Science.* 2017;358(6367):eaan4368.
- Reinecke M, Ruprecht B, Poser S, Wiechmann S, Wilhelm M, Heinzlmeir S, et al. Chemoproteomic selectivity profiling of PI3K and PI3K kinase Inhibitors. *ACS Chem Biol.* 2019;14(4):655–64.
- Bantscheff M, Eberhard D, Abraham Y, Bastuck S, Boesche M, Hobson S, et al. Quantitative chemical proteomics reveals mechanisms of action of clinical ABL kinase inhibitors. *Nat Biotechnol.* 2007;25(9):1035–44.
- Wiechmann S, Ruprecht B, Siekmann T, Zheng R, Frejino M, Kunold E, et al. Chemical phosphoproteomics sheds new light on the targets and modes of action of AKT inhibitors. *ACS Chem Biol.* 2021;16(4):631–41.
- Li S, Shen D, Shao J, Crowder R, Liu W, Prat A, et al. Endocrine-therapy-resistant ESR1 variants revealed by genomic characterization of breast-cancer-derived xenografts. *Cell Rep.* 2013;4(6):1116–30.
- Saltzman AB, Leng M, Bhatt B, Singh P, Chan DW, Dobrolecki L, et al. gpGroupier: a peptide grouping algorithm for gene-centric inference and quantitation of bottom-up proteomics data. *Mol Cell Proteomics MCP.* 2018;17(11):2270–83.
- Perkins DN, Pappin DJ, Creasy DM, Cottrell JS. Probability-based protein identification by searching sequence databases using mass spectrometry data. *Electrophoresis.* 1999;20(18):3551–67.
- Käll L, Canterbury JD, Weston J, Noble WS, MacCoss MJ. Semi-supervised learning for peptide identification from shotgun proteomics datasets. *Nat Methods.* 2007;4(11):923–5.
- MacLean B, Tomazela DM, Shulman N, Chambers M, Finney GL, Frewen B, et al. Skyline: an open source document editor for creating and analyzing targeted proteomics experiments. *Bioinforma Oxf Engl.* 2010;26(7):966–8.
- Stopfer LE, Gajadhar AS, Patel B, Gallien S, Frederick DT, Boland GM, et al. Absolute quantification of tumor antigens using embedded mhc-i isotopologue calibrants. *Proc Natl Acad Sci U S A.* 2021. <https://doi.org/10.1073/pnas.2111173118>.
- Matsunuma R, Chan DW, Kim BJ, Singh P, Han A, Saltzman AB, et al. DPYSL3 modulates mitosis, migration, and epithelial-to-mesenchymal transition in claudin-low breast cancer. *Proc Natl Acad Sci U S A.* 2018;115(51):E11978–87.
- Huang KL, Li S, Mertins P, Cao S, Gunawardena HP, Ruggles KV, et al. Proteogenomic integration reveals therapeutic targets in breast cancer xenografts. *Nat Commun.* 2017;8:14864.
- Chartier M, Chénard T, Barker J, Najmanovich R. Kinome Render: a stand-alone and web-accessible tool to annotate the human protein kinome tree. *PeerJ.* 2013;1:e126.
- Nguyen DT, Mathias S, Bologna C, Brunak S, Fernandez N, Gaulton A, et al. Pharos: collating protein information to shed light on the druggable genome. *Nucleic Acids Res.* 2017;45:D995–1002.
- Meric-Bernstam F, Johnson A, Holla V, Bailey AM, Brusco L, Chen K, et al. A decision support framework for genomically informed investigational cancer therapy. *J Natl Cancer Inst.* 2015. <https://doi.org/10.1093/jnci/djv098>.
- Parker JS, Mullins M, Cheang MCU, Leung S, Voduc D, Vickery T, et al. Supervised risk predictor of breast cancer based on intrinsic subtypes. *J Clin Oncol.* 2009;27(8):1160–7.



29. Pu M, Messer K, Davies SR, Vickery TL, Pittman E, Parker BA, et al. Research-based PAM50 signature and long-term breast cancer survival. *Breast Cancer Res Treat.* 2020;179(1):197–206.
30. Pommier RM, Sanlaville A, Tonon L, Kielbassa J, Thomas E, Ferrari A, et al. Comprehensive characterization of claudin-low breast tumors reflects the impact of the cell-of-origin on cancer evolution. *Nat Commun.* 2020;11(1):1–12.
31. Fougner C, Bergholtz H, Norum JH, Sørbye T. Re-definition of claudin-low as a breast cancer phenotype. *Nat Commun.* 2020;11(1):1–11.
32. Nusinow DP, Szpyt J, Ghandi M, Rose CM, McDonald ER, Kalocsay M, et al. Quantitative proteomics of the cancer cell line encyclopedia. *Cell.* 2020;180(2):387–402.e16.
33. Olson JA, Budd GT, Carey LA, Harris LA, Esserman LJ, Fleming GF, et al. Improved surgical outcomes for breast cancer patients receiving neoadjuvant aromatase inhibitor therapy: results from a multicenter phase II trial. *J Am Coll Surg.* 2009;208(5):906–14.
34. Satpathy S, Jaehnig EJ, Krug K, Kim BJ, Saltzman AB, Chan DW, et al. Microscaled proteogenomic methods for precision oncology. *Nat Commun.* 2020;11(1):1–16.
35. Yoshihara K, Shahmoradgoli M, Martínez E, Vegesna R, Kim H, Torres-García W, et al. Inferring tumour purity and stromal and immune cell admixture from expression data. *Nat Commun.* 2013;4(1):1–11.
36. Carter SL, Cibulskis K, Helman E, McKenna A, Shen H, Zack T, et al. Absolute quantification of somatic DNA alterations in human cancer. *Nat Biotechnol.* 2012;30(5):413–21.
37. Kennedy JJ, Whiteaker JR, Kennedy LC, Bosch DE, Lerch ML, Schoenherr RM, et al. Quantification of human epidermal growth factor receptor 2 by immunopeptide enrichment and targeted mass spectrometry in formalin-fixed paraffin-embedded and frozen breast cancer tissues. *Clin Chem.* 2021;67(7):1008–18.
38. Perez-Riverol Y, Bai J, Bandla C, García-Seisdedos D, Hewapathirana S, Kamatchinathan S, et al. The PRIDE database resources in 2022: a hub for mass spectrometry-based proteomics evidences. *Nucleic Acids Res.* 2022;50(D1):D543–52.
39. Chen P, Lee NV, Hu W, Xu M, Ferre RA, Lam H, et al. Spectrum and degree of CDK drug interactions predicts clinical performance. *Mol Cancer Ther.* 2016;15(10):2273–81.

## Publisher's Note

Springer Nature remains neutral with regard to jurisdictional claims in published maps and institutional affiliations.

Ready to submit your research? Choose BMC and benefit from:

- fast, convenient online submission
- thorough peer review by experienced researchers in your field
- rapid publication on acceptance
- support for research data, including large and complex data types
- gold Open Access which fosters wider collaboration and increased citations
- maximum visibility for your research: over 100M website views per year

At BMC, research is always in progress.

Learn more [biomedcentral.com/submissions](https://biomedcentral.com/submissions)

